DOI: 10.24996/ijs.2026.67.8.22

ISSN: 0067-2904

Influence of gas flow rate on spectroscopic characterization of Cu-Zn Alloy plasma by OES

Mohammed H. Jawad [*], Mohammed R. abdulameer

Department of Physics , College of Science , University of Baghdad Iraq

Received: 15/ 2/2025 Accepted: 3/ 9 /2025 Published: 30/ 8/2026

Abstract:

In this work, a plasma jet system generated in a deionized aqueous medium was studied. A locally manufactured copper-zinc alloy with a ratio of 80:20 was used for this purpose, and a bidirectional power supply with a total output of 20 kV and a cutoff frequency of 30 kHz was used. The gas flow rate was varied at 3, 3.5, 4, 4.5, and 5 liters per minute (L/min) while the voltage was kept constant at 13 kV. The emission lines of the copper-zinc alloy elements and gases were determined in the range of 200 to 1000 nm. Key plasma parameters, such as the particle number in the Debye sphere, plasma frequency, and Debye length, as well as the most important parameters, such as electron density and temperature, were then calculated. The study concluded that increasing the gas flow rate increased the plasma emission. The maximum peak for argon gas under the operating conditions used at the highest flow value was 811.5311 nm. Alloy element emissions appeared in the wavelengths between 200 and 300 nm. A decrease in electron temperature was observed with increasing gas flow rate, reaching its highest value at the highest gas flow rate used, reaching 0.703 eV. In contrast, a clear increase in electron density was observed with increasing gas flow rate. This behavior indicates that the interaction between the plasma and the surrounding environment, as well as the ionization dynamics, strongly depends on the gas flow rate. These results provide valuable insights into the role of flow rate in shaping plasma properties such as emission intensity, as well as temperature and electron density, which are critical for improving the performance of plasma-based applications.

Keywords: Zn-Cu Alloy plasma, Optical spectroscopy of plasma (OES), Plasma properties and parameters.

تأُثير معدل تدفق الغاز على التوصيف الطيفي لبلازما سبيكة نحاس – زنك باستخدام طريقة OES

محمد حمزة جواد[*]، محمد رضا عبد الامير

قسم الفيزياء، كلية العلوم، جامعة بغداد، بغداد، العراق

الخلاصة

[*] Email : mohammed.hamza1204a@sc.uobaghdad.edu.iq

في هذا العمل، تمت دراسة نظام نفث البلازما المُولّد في وسط مائي منزوع الأيونات. استُخدمت سبيكة نحاس–زنك مُصنّعة محليًا بنسبة 20:80 لهذا الغرض، ومصدر طاقة ثنائي الاتجاه بإجمالي خرج 20 كيلو فولت وتردد قطع 30 كيلو هرتز. تراوحت معدلات التدفق المستخدمة في التجربة بين 3 و3.5 و4 و4.5 و5 لترات في الدقيقة (لتر/دقيقة) وتم تثبيت الجهد عند 13 كيلو فولت. حُدّدت خطوط انبعاث عناصر وغازات سبيكة النحاس–الزنك في نطاق 200 إلى 1000 نانومتر. ثم حُسبت معلمات البلازما الرئيسية، مثل طول ديباي وتردد البلازما وعدد الجسيمات في كرة ديباي، بالإضافة إلى أهم المعلمات، مثل كثافة الإلكترونات ودرجة الحرارة. وخلصت الدراسة إلى أن زيادة معدل تدفق الغاز تزيد من انبعاث البلازما. بلغ الحد الأقصى لذروة غاز الأرجون في ظل ظروف التشغيل المستخدمة عند أعلى قيمة تدفق 811.5311 نانومتر. وظهرت انبعاثات عناصر السبائك في نطاق الطول الموجي 200–300 نانومتر. ولوحظ انخفاض في درجة حرارة الإلكترون مع زيادة معدل التدفق، ليصل إلى أعلى قيمة له عند أعلى معدل تدفق للغاز المستخدم، حيث بلغ 0.703 إلكترون فولت. في المقابل، لوحظت زيادة واضحة في كثافة الإلكترونات مع زيادة التدفق. يشير هذا السلوك إلى أن التفاعل بين البلازما والبيئة المحيطة، بالإضافة إلى ديناميكيات التأين، يعتمد بشدة على معدل تدفق الغاز. توفر هذه النتائج رؤى قيّمة حول دور معدل التدفق في تشكيل خصائص البلازما، مثل شدة الانبعاث وكثافة الإلكترونات ودرجة الحرارة، وهي عوامل بالغة الأهمية لتحسين أداء التطبيقات القائمة على البلازما.

Introduction

Non-thermal and low-temperature plasma is one of the topics that is of great importance at present due to its wide applications in various fields. Many low-temperature plasma systems at atmospheric pressure have been developed so far [1-3]. Plasma jetting is one of the most important methods for generating plasma at atmospheric pressure. This method has wonderful characteristics, the most important of which is the low operating cost and the ability to generate electrons at high temperatures compared to molecules and ions, in addition to its ability to cause important chemical reactions used in medical and industrial applications [4]. One of the interesting properties of plasma jets at atmospheric pressure is that they have a great ability to infiltrate and spread inside narrow spaces, such as openings and tubes, which facilitates their use in many fields [5,6]. These facts consider plasma jetting to be of wide interest and very attractive in the medical and biological field, as the process of forming plasma and its flow inside narrow tubes is useful in delivering it to specific places, which is considered very important in endoscopic medical applications, such as cancer treatment, colon, rectum, and pancreas [7,8].

The plasma jetting technology used in this study is considered one of the most promising and new technologies used in the process of generating glowing and cold plasma at atmospheric pressure. This plasma, which is generated at atmospheric pressure, is used in many industrial, medical, and biological applications, including the science of polymerization and surface modification of various types of materials. It is also used in air treatment technologies, pollutant removal, water purification, and treatment of various gas states [9].

Various spectroscopic methods, including optical emission spectroscopy (OES), calculate the radiation emitted by the plasma because this radiation represents the properties of the plasma produced in the surrounding area [10]. Electrons interact with particles due to their high speeds, resulting in numerous collisions and excitations. These collisions and interactions result in the emission of radiation in three forms: line spectrum, band spectrum, or continuum spectrum. When electrons move between different energy levels within an atom, ions and atoms emit radiation. Unlike continuous radiation, such as bremsstrahlung radiation, this radiation is emitted in the form of short, distinct spectral waves [11-12]. The process of diagnosing plasma is done by calculating the temperature of the electrons and their heat, and also determining the distribution of the amount of energy that affects the temperature of the resulting plasma according to the temperature, as the definition of the state of thermal equilibrium of the plasma is based on the density of electrons[13]. The temperature of the electrons is calculated using Boltzmann plot [14]according to the equation:

$$\ln\left[\frac{\lambda_{ji}I_{ji}}{hcA_{ji}g_j}\right] = \frac{1}{\mathrm{k_B T}}\left(E_j\right) + \ln\left[\frac{\mathrm{N}}{\mathrm{U(T)}}\right] \quad \dots\dots\dots\dots(1)$$

I_{ji} refers to the intensity of the spectral lines between the two levels, while g_j represents the statistical weight of the highest energy level. Meanwhile, E_j refers to the excitation energy and A_{ji} the transition probability. A free line of self-absorption is necessary for the Stark broadening effect to detect the electron density [15].

$$n_e = \left(\frac{\Delta\lambda_{FWHM}}{2w}\right)N_r \quad \dots\dots\dots\dots\dots(2)$$

w is the Stark broadening parameter for the theoretical line full width, and Nr is the reference electron density typically taken as approximately≈1017 cm-3, [16,17].

Debye's length can be computed using the following formula[16,17]:

$$\lambda_D = \left[\frac{\varepsilon_o K_B T_e}{n_e e^2}\right]^{1/2} \cong 7.43\times10^2\left(\frac{T_e(e\,\mathrm{V})}{n_e}\right)^{\frac{1}{2}} \quad \dots\dots\dots\dots\dots(3)$$

While the frequency of the plasma can be calculated by [18]:

$$\omega_{pe} = \left(n_e e^2/m_e\varepsilon_0\right)^{\frac{1}{2}} \quad \dots\dots\dots\dots\dots(4)$$

where ε_o Is the permittivity and m_e is the electron mass.

1. Materials and Methods

1.1 Preparation of Cu-Zn Alloy and Main Tools

A locally made Cu-Zn alloy piece measuring 10 cm x 10 cm with a composition ratio of 80:20 was prepared by the gas furnace casting method to ensure the best homogeneity between the components. A section of 6 cm in length, 1.5 cm in width, and 3 mm in thickness was cut from this alloy and immersed in deionized water, after which it was placed in a small beaker.

To generate plasma, argon gas and a high-voltage power source with a total output of 20 kV were used. In this experiment, the voltage was set at a constant value of 13 kV. The central units involved in controlling the current plasma jet system are the gas flow unit and the voltage control unit. At atmospheric pressure, the argon gas is ionized, and plasma is generated. The negative terminal (cathode) of the voltage source is connected to the plasma jet terminal, and the anode terminal is connected to the target alloy, as shown in Figure 1.
During the plasma generation process, the voltage was fixed at 13 kV. The process of controlling the length of the plasma column was done by changing the gas flow rate (measured using a mechanical-tube rotameter flowmeter) at (3, 3.5, 4, 4.5, and 5 L/min). For each of these gas flow rates, the effect of the applied voltage on the plasma length was studied by changing the applied voltage at (5, 7, 9, 11, 13 kV).

The diagnostics were performed in the laboratory under atmospheric room pressure. A spectrometer (type S3000-UV-NIR) was installed near the plasma jet resulting from the alloy and argon gas, Emission readings were taken in the range of 200 to 1000 nanometers during plasma generation. The recorded data were then examined and compared with the data provided by the National Institute of Standards and Technology (NIST). And the plasma parameters were computed.

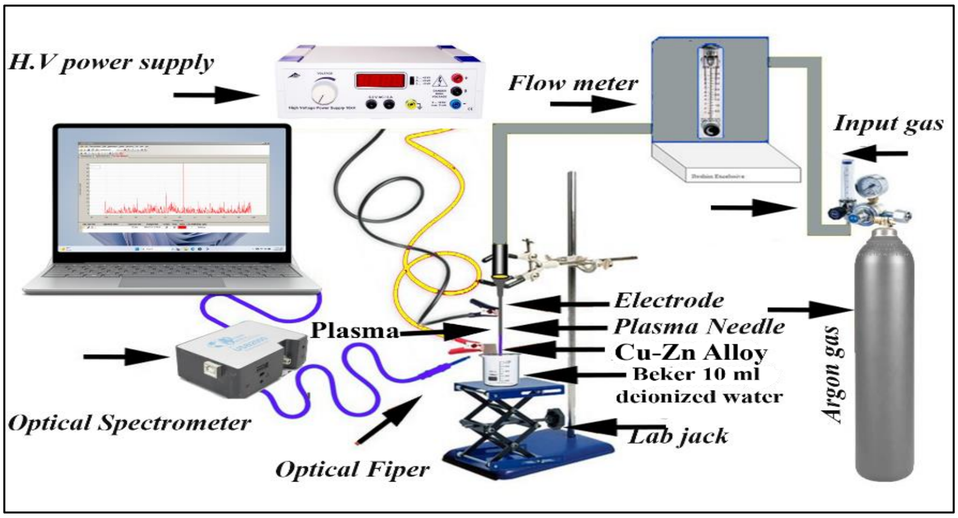

Figure 1: Atmospheric plasma jet system with spectrometer and control unit

2. Results and Discussion

Figure 2 displays the intensity distribution spectra derived from the diagnosis at a steady 13 kV applied voltage and various gas flow rates (3-5 liters per minute).

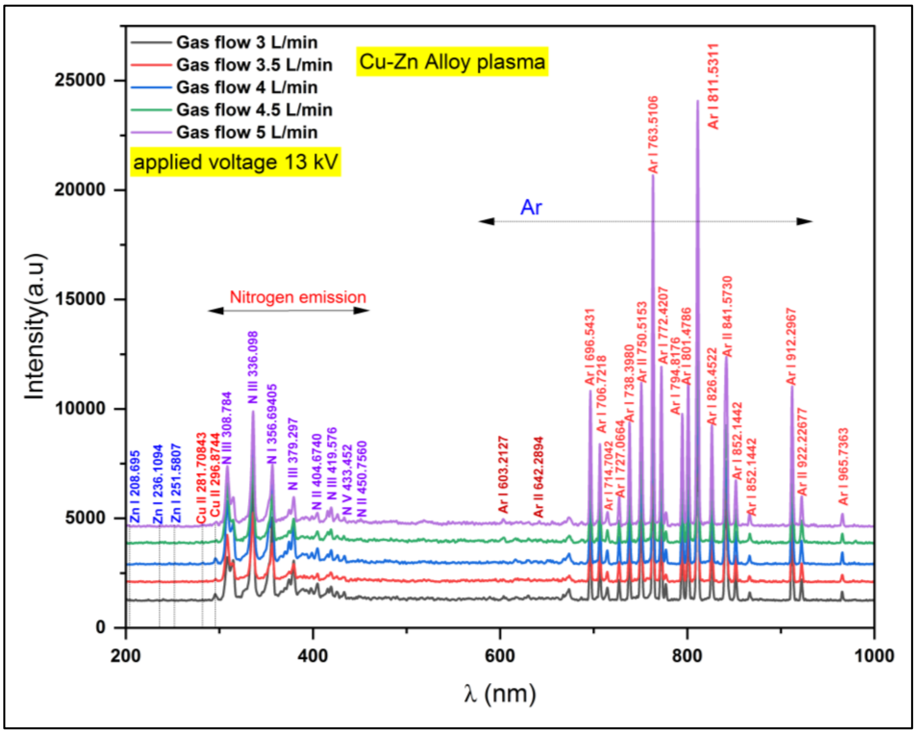

Figure -2: The intensity distributions spectra at a fixed voltage of 13 kV and different gas flow rates

Several peaks were recorded in the argon spectrum and compared with the National Institute of Standards and Technology's global data, which was used in the diagnostic calculations [19]. The argon spectrum peaks were consistent with the above-mentioned NIST data. The highest peak for argon appeared at 811.5311 nm for all gas flow rates. On the other hand, nitrogen emission peaks appeared in the range 308 to 450 nm, and the highest peak recorded for this gas was at 336.098 nm at a gas flow rate of 5 liters per minute. Most of the produced plasma peaks appeared in the wavelength range 200 to 1000 nm. An apparent increase in the peaks intensity occurred with increasing the gas flow rate. The reason for this increase is the increase of plasma interactions as the gas flow rate increased [20]. Additionally, the figure displays the active plasma types that emerged under these circumstances.

A portion of Figure 2 has been cropped within the spectral emission range, as shown in Figure 3, to illustrate the emissions of these elements during the plasma generation process. The emissions of zinc and copper appeared within the range (200 to 300 nm) at a voltage value of 13 kV and a variable gas flow rate. The highest peak of zinc emission was at a wavelength of 251.5807 nm, while the highest peak of copper emission was at a wavelength of 281.7043 nm.

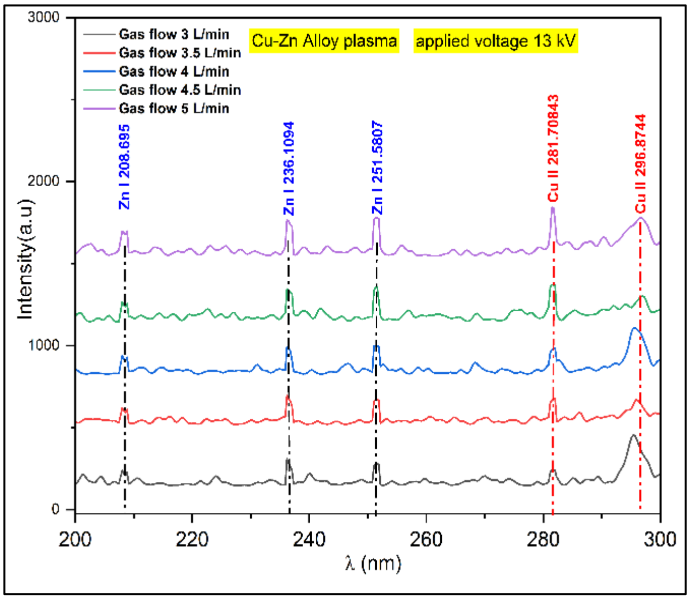

Figure 3: Discrimination of the intensity of alloy metals (cu -zn) as a function of wavelength for different values of flow.

The Boltzmann plot method was used to calculate the electron temperature based on Equation 1 by drawing the relationship between ($\ln\left[\frac{\lambda_{ji} I_{ji}}{hcA_{ji}g_j}\right]$) and E_j. The reciprocal of the slope represents the electron temperature, as shown in Figure 4. The R^2 value represents the statistical fit coefficient, which indicates how well the linear data fit. Its accuracy increases as it approaches 1. Table 1 represents the use of five spectral lines extracted from the National Institute of Standards and Technology.

Table 1: Spectral emission parameters of emitting plasmas consistent with the NIST database

Spectral lines	λ (nm)	A_{ij} (s^{-1})	EK (eV)	Transitions
Ar I	696.5431	1.90E+07	13.32785705	$3s^23p^5(^2P°_{3/2})4s$ ⟶ 3s23p5(2P°$_{1/2}$)4p
	706.7218	1.90E+07	13.30222747	3s23p5(2P°$_{3/2}$)4s ⟶ 3s23p5(2P°$_{1/2}$)4p
	738.398	4.20E+07	13.30222747	3s23p5(2P°$_{3/2}$)4s ⟶ 3s23p5(2P°$_{1/2}$)4p
	763.5106	1.22E+08	13.1717777	3s23p5(2P°$_{3/2}$)4s ⟶ 3 s23p5(2P°$_{3/2}$)4p
	811.5311	2.30E+08	13.07571571	3s23p5(2P°$_{3/2}$)4s ⟶ 3s23p5(2P°$_{3/2}$)4p

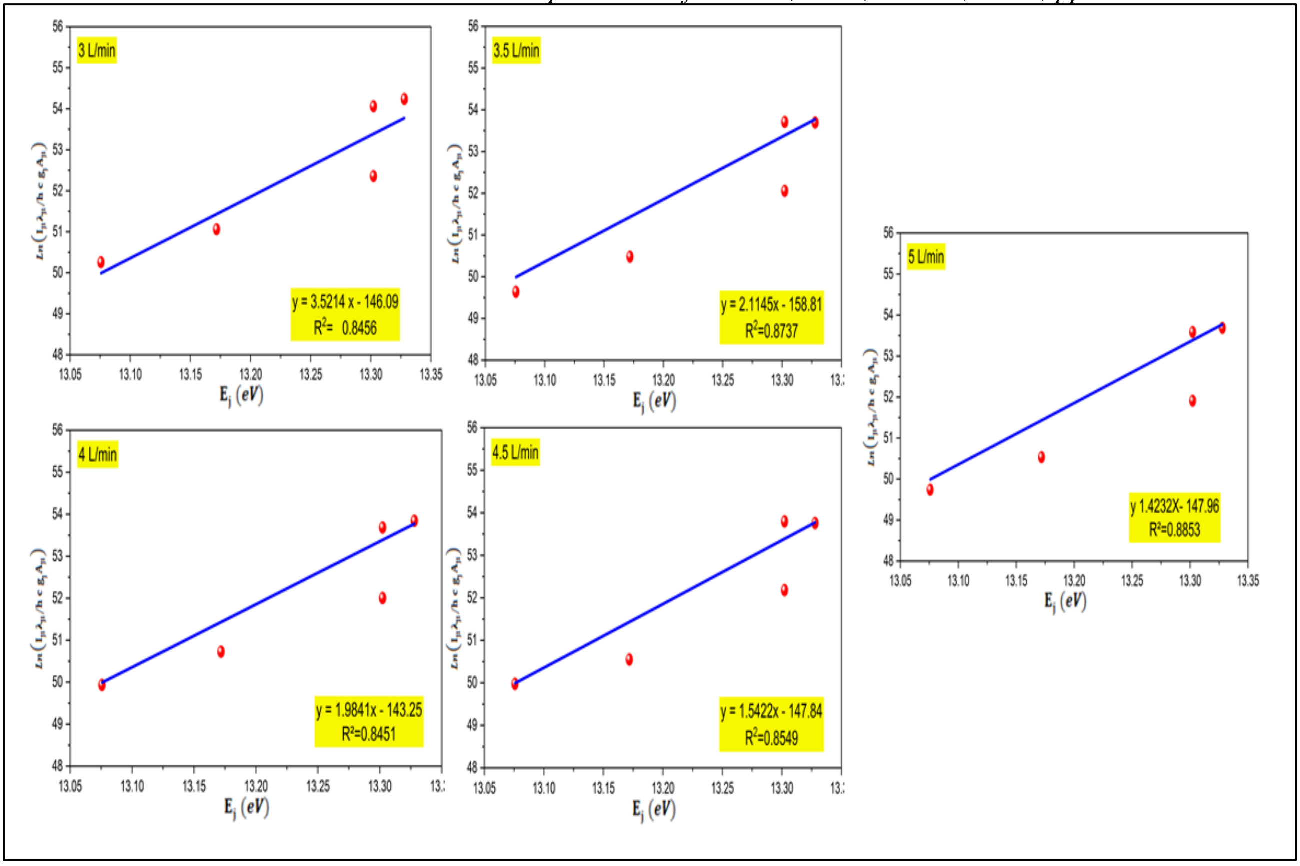

Figure 4: Boltzmann plots for different gas flow rates at a constant applied voltage of 13 kV.

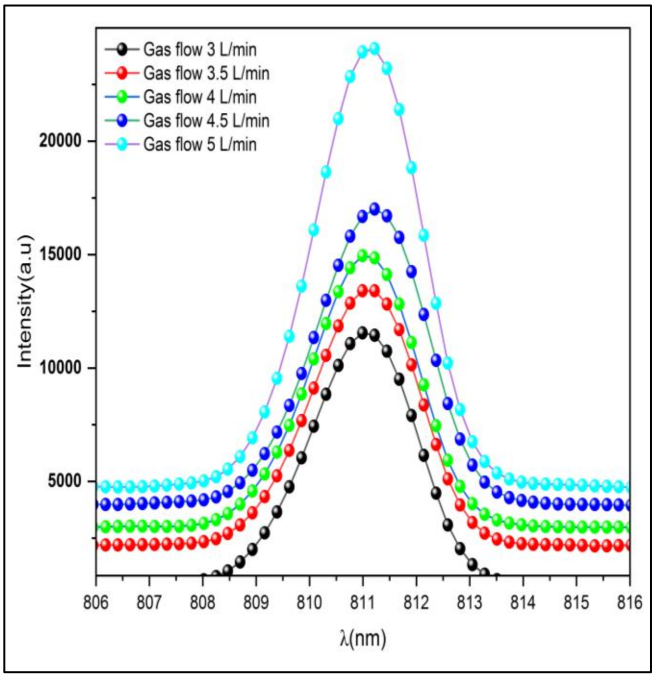

Figure 5: The highest peak wavelength used in the electron density calculation for different gas flow rates.

Table 2 shows the plasma parameters measured at different gas flow rates with a constant applied voltage value of 13 kV. These parameters were calculated using Equations (1-4). The table shows that as gas flow rate increases, the Debye length decreases, and the measured plasma frequency increases.

Table 2: Measurements of the atmospheric plasma jet's characteristics at various gas flow rates.

Gas flow (L/min)	*FWHM (nm)*	T_e (eV)	n_e*10^{17} (cm^{-3})	f_p*10^{12} (Hz)	λ_D*10^{-6} (cm)	N_d*10^3
3	2.26	0.703	1.38	1.053	5.31	8.6
3.5	2.32	0.648	1.41	1.067	5.04	7.5
4	2.38	0.504	1.45	1.081	4.38	5.1
4.5	2.42	0.473	1.47	1.09	4.21	4.60
5	2.54	0.284	1.55	1.116	3.19	2.09

Figure 6 shows the relationship between the electron density and temperature with the change in the gas flow rate used to generate the plasma. It is clear that the temperature decreased from 0.284 to 0.703 eV with increasing the gas flow rate; and the density increased from $1.38*10^{17}cm^{-3}$ to $1.55*10^{17}cm^{-3}$. The collision rate of electrons and argon gas molecules increases with increasing gas flow rate, which increases the process of transferring energy to the electrons and thus increases the energy of the gas and as a result increases the density and decreases the temperature of the electrons. The ionization process that occurs as a result of the collisions enhances this effect. In addition, the spread of charged particles towards the walls of the tube leads to the loss of these particles, but the cylindrical shape of the tube balances the collisions inside the plasma. Thus a regular increase in the electron density appears, as shown in Figure 6, which is consistent with a previous study of Abbas and Aadim [21].

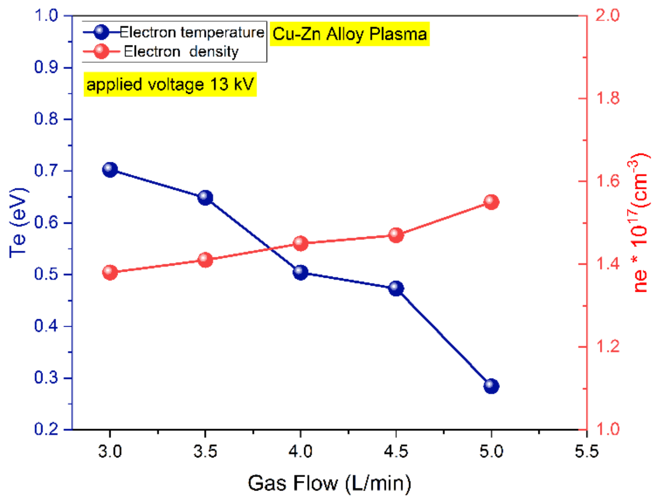

Figure 6: The electron temperature (T_e) and number density (ne) in a Cu-Zn alloy plasma jet at variable flow rate (3,3.5,4,4.5,5 L/min) and a constant

Figure 7a and 7b show the change in Debye length, plasma frequency, and Debye number as a function of the change in gas flow rate, respectively. The plasma frequency increases with increasing gas flow rate, indicating an increase in the electron density in the system. In contrast, the Debye length gradually decreases with increasing gas flow, indicating a decrease in charge influence. The Debye number reflects an apparent decrease as the gas flow rate increases, indicating improved plasma stability and enhanced electrostatic shielding.

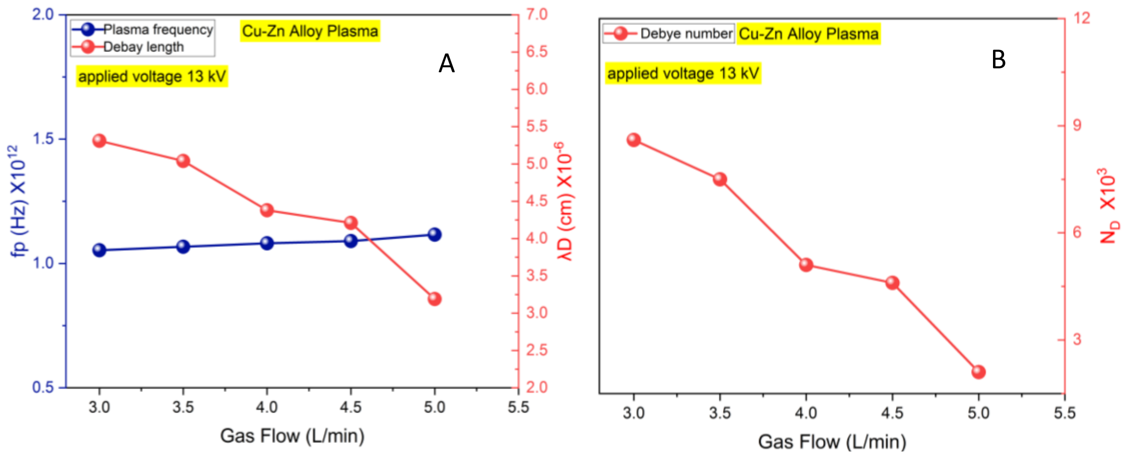

Figure 7: (a)variation in plasma frequency and Debye length as a function of gas flow rate, (b) variation in Debye number as a function of gas flow rate

Figure 8 shows the plasma length as a function of applied voltage and gas flow. Since plasma is a gas charged with high energy, the figure below shows how this energy changes and expands based on changing the voltage intensity and gas flow rate per minute.

If the gas flow rate is increased, the plasma begins to expand more because the gas pushes the plasma forward. On the other hand, increasing the voltage applied to the system increases the plasma length more because the high voltage provides more energy to the molecules, and they become more able to spread. The highest plasma length was recorded at a voltage of 13 kilovolts and a gas flow rate of 5 liter per minute, where the plasma length reached 3 cm. The shortest plasma length was 1.1 cm at a gas flow of 3 L/min. note that the increase between these two variables causes the plasma length to increase gradually. It was also noted that the voltage has a greater effect on improving the plasma length. The higher the voltage, the longer the plasma length.

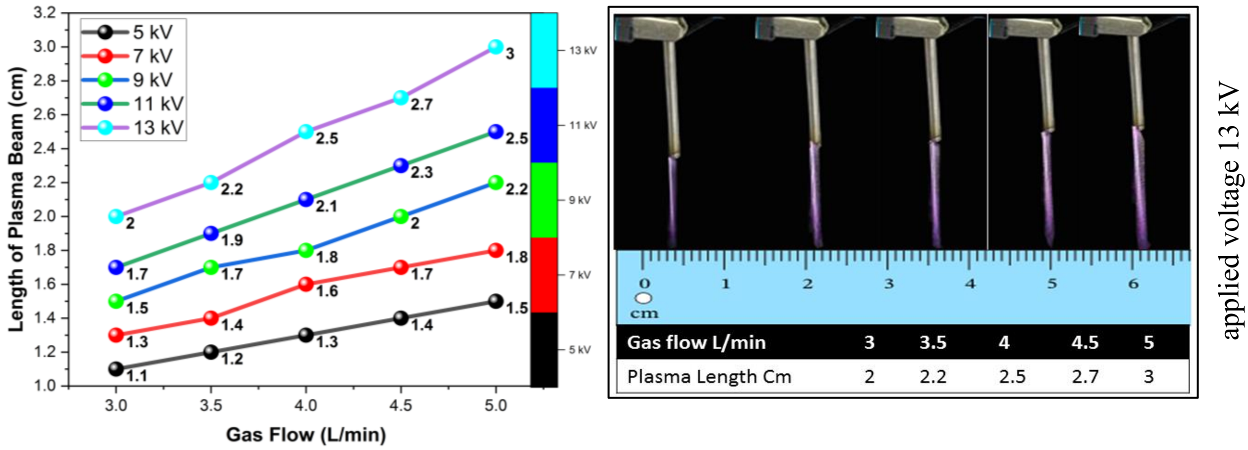

Figure 8: plasma length with respect to change in gas flow and voltage.

3. Conclusions

It was found that the emission lines of zinc and copper alloys depend primarily on external variables imposed on the system, such as the gas flow rate and the applied voltage. This study concluded that raising the argon gas flow rate would lead to a significant increase in emission intensity, attributed to the increased collision frequency that would increase with increasing flow, directly affecting the ionization rate and excitation associated with the jet plasma generation process. The results showed that the highest emission peak for Zn was at 251.5807 nm at a flow rate of 5 L/min, while the lowest peak for Zn was at 208.965 nm. Meanwhile, the highest peak for copper was at 281.7043 nm, while the lowest value was at 296.8744 nm. The results indicated that an increase in the gas flow rate was accompanied by an increase in the spectral emission intensity of the alloy's constituent metals. This increase affected key plasma parameters, such as electron temperature and density, as well as an increase in both the plasma frequency and Debye length, and the number of charged particles in the Debye field. In addition to these results, it was concluded that this system is capable of successfully generating plasma up to 3 cm in length, with a flow rate of 5 L/min at an applied voltage of 13 kV, enabling its use in many important applications.

Acknowledgment

Thanks to the Physics Department at the University of Baghdad, College of Science, and to the Plasma Laboratory for Postgraduate Studies for their support in completing this work.

References

[1] Z. Hubicka *et al.*, “Barrier-torch discharge plasma source for surface treatment technology at atmospheric pressure,” *Plasma Sources Science and Technology.*, vol. 11, no. 2, p. 195, 2002.

[2] M. H. Jawad and M. R. Abdulameer, “The effect of background argon gas pressure on parameters of plasma produced by DC- glow discharge,” *Iraqi Journal of Science.*, vol. 64, no. 3, pp. 1210–1218, 2023, doi: 10.24996/ijs.2023.64.3.17.

[3] M. A. Lieberman and A. J. Lichtenberg, “Principles of plasma discharges and materials processing,” *MRS Bulletin.*, vol. 30, no. 12, pp. 899–901, 1994.

[4] K. A. Aadim and G. H. Jihad, “Determination of Electrons Temperature and Density For Ag, Zn, and Cu metals using Plasma jet System at atmospheric pressure,” *Iraqi Journal of Science.*, vol. 63, no. 5, pp. 2039–2047, 2022, doi: 10.24996/ijs.2022.63.5.19.

[5] R. Zaplotnik, G. Primc, and A. Vesel, “Optical emission spectroscopy as a diagnostic tool for characterization of atmospheric plasma jets,” *Applied Sciences.*, vol. 11, no. 5, p. 2275, 2021.

[6] M. M. Shehab and K. A. Aadim, “Spectroscopic diagnosis of the CdO:CoO plasma produced by Nd:YAG laser,” *Iraqi Journal of Science.*, vol. 62, no. 9, pp. 2948–2955, 2021, doi: 10.24996/ijs.2021.62.9.11.

[7] E. Stoffels, “‘Tissue processing’ with atmospheric plasmas,” *Contributions to Plasma Physics.*, vol. 47, no. 1-2, pp. 40–48, 2007.

[8] Z. T. Turki, M. Fahem, Z. A. Mankhi, and M. H. Jawad, “Magnetic field effect on cadmium oxide plasma properties detected by laser spectroscopy,” *Russian Physics Journal.*, pp. 1–9, 2025.

[9] Abbas, Z.M., Abbas, Q.A. Aluminum-doped ZnO nano-laminar structures by pulsed laser ablation for gas sensing application. J Opt 53, 544–557 (2024).

[10] D. A. Cremers and L. J. Radziemski, *Handbook of laser-induced breakdown spectroscopy*. *John Wiley & Sons (Book Publisher)*, 2013.

[11] K. Hoppstock and W. W. Harrison, “Spatial distribution of atoms in a dc glow discharge,” *Analytical Chemistry.*, vol. 67, no. 18, pp. 3167–3171, 1995.

[12] Q. A. Abbas, “Diagnostics of dusty plasma properties in planar magnetron sputtering device,” *Iraqi Journal of Physics*., vol. 13, no. 26, pp. 64–75, 2019,

[13] H. R. Humud, “Effect of plasma jet on the water and hydrogen peroxide that used for assisted teeth bleaching,”*Iraqi Journal of Physics.*, vol. 15, no. 34, pp. 29–35, 2019, doi: 10.30723/ijp.v15i34.117.

[14] R. F. G. Meulenbroeks, M. F. M. Steenbakkers, Z. Qing, M. C. M. Van de Sanden, and D. C. Schram, “Four ways to determine the electron density in low-temperature plasmas,” *Physical Review E*, vol. 49, no. 3, p. 2272, 1994.

[15] T. A. Hameed and H. R. Humud, “Comparison Study of Plasma-Activated Water and Plasma Jet Effects on Escherichia coli Bacteria for the Disinfection of Tooth Root Canal,” Iraqi Journal of Science., vol. 64, no. 12, pp. 6285–6293, 2023,

[16] R. T. Ahmed, A. F. Ahmed, and K. A. Aadim, “Influence of laser energy on structural and morphology properties of CdO and CdO: Sn production by laser-induced plasma,” *Journal of Optics.*, vol. 53, no. 2, pp. 1564–1573, 2024.

[17] K. Behringer and U. Fantz, “Spectroscopic diagnostics of glow discharge plasmas with non-Maxwellian electron energy distributions,” *Journal of Physics D: Applied Physics.*, vol. 27, no.

10, p. 2128, 1994.

[18] Kadhem, S. J. (2023). Preparation of Al2O3/PVA nanocomposite thin films by a plasma jet method. Science and Technology Indonesia, 8(3), 471-478.

[19] K. A. Aadim and A. H. Khidhir, "Effect of Zinc (Zn)-Doped on the Structural, Optical and Electrical Properties of (Cdo) 1-Xznx Films Prepared by Pulsed Laser Deposition Technique," *Iraqi Journal of Physics.*, vol. 19, no. 51, pp. 64–71, 2021.

[20] R. K. Tyagi, R. S. Pandey, A. Kumar, and K. K. Srivastava, "Effect of electric and magnetic field on welding parameters in plasma welding," *International Journal of Engineering Science and Technology.*, vol. 3, no. 8, pp. 168–176, 2011.

[21] I. K. Abbas and K. A. Aadim, "Spectroscopic Diagnosis of Cobalt Plasma Produced by OES Technique and Influence of Applied Voltage on Plasma Parameters,"*Iraqi Journal of Science.*, vol. 64, no. 5, pp. 2271–2281, 2023, doi: 10.24996/ijs.2023.64.5.15.